KSTLE International Journal, Vol. 2, No. 1, June 2001, pp. 12-16

Finite Element Analysis of Multiple Subsurface Cracks in Half-space Due to Sliding Contact

Sang Yun Lee and Seock Sam Kim*,†

Graduate School, Department of Mechanical Engineering, Kyungpook National University, Taegu 702-701, South Korea
**School of Mechanical Engineering, Kyungpook National University, Taegu 702-701, South Korea*

Abstract : A finite element analysis of crack propagation in a half-space due to sliding contact was performed. The sliding contact was simulated by a rigid asperity moving across the surface of an elastic half-surface containing single and multiple cracks. Single, coplanar, and parallel cracks were modeled to investigate the interaction effects on the crack growth in contact fatigue. The analysis was based on linear elastic fracture mechanics and the stress intensity factor concept. The crack propagation direction was predicted based on the maximum range of the shear and tensile stress intensity factors.

Key words : Fracture mechanics, finite element method, stress intensity factor, multiple crack

Introduction

It is well known that the initiation and nucleation of microcracks or microvoids and crack propagation or void growth occur due to normal and tangential traction. The wear particles are generated when the process of wear particle formation by subsurface deformation, crack nucleation, and crack propagation is completed, as postulated by the delamination theory of wear [1-3]. Since the delamination theory was proposed, there have been many studies about horizontal subsurface cracks.

H. Salehizadeh reported that in the case of a subsurface horizontal crack, the mode II stress intensity factor KII is greater than the mode I stress intensity factor KI [4]. S. Jayaraman studied the crack propagation direction of a branched crack [5]. Komvopoulos reported that subsurface crack growth due to moving surface traction is essentially a fatigue process, therefore, the determination of the crack propagation directions must be based on the corresponding maximum stress intensity factor ranges [6].

The works reviewed so far have dealt with single cracks. However, real engineering materials have many subsurface cracks and these cracks interact with each other.

Accordingly, this paper considers multiple subsurface cracks under sliding contact conditions. The main objective of the present analysis is to examine the interaction of multiple cracks.

Modeling Procedures

Statement of Problem

The contact of two surfaces in relative motion can be viewed as the microcontacting of asperities. As a result, this three-dimensional contact problem can be simplified into a two-dimensional plane-strain problem of cylindrical asperites in contact with a semi-infinite half-space which have a coplanar crack and parallel crack, as shown schematically in Fig. 1. The radius of a rigid cylindrical asperity was set at 25 μm and it was assumed to slide over a cracked half-space with an

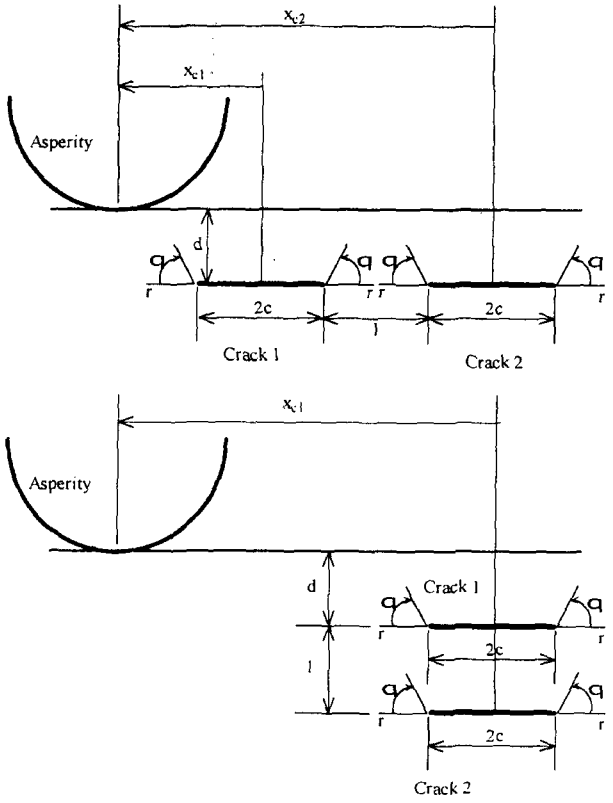

Fig. 1. Schematic representation of contact.

†Corresponding author; Tel: 82-53-950-5577; Fax: 82-53-950-6588
E-mail: sskim@knu.ac.kr

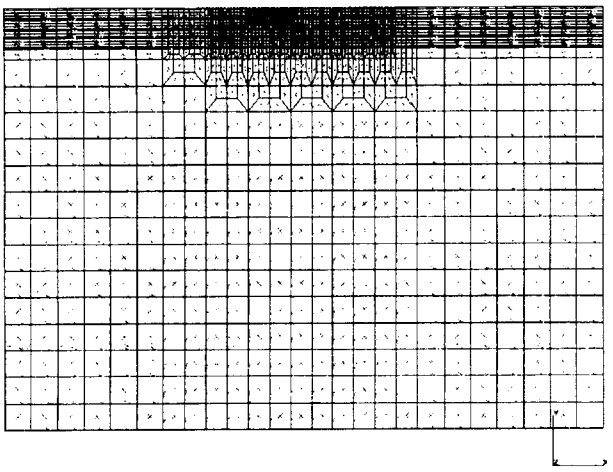

Fig. 2. Finite element mesh of half-space.

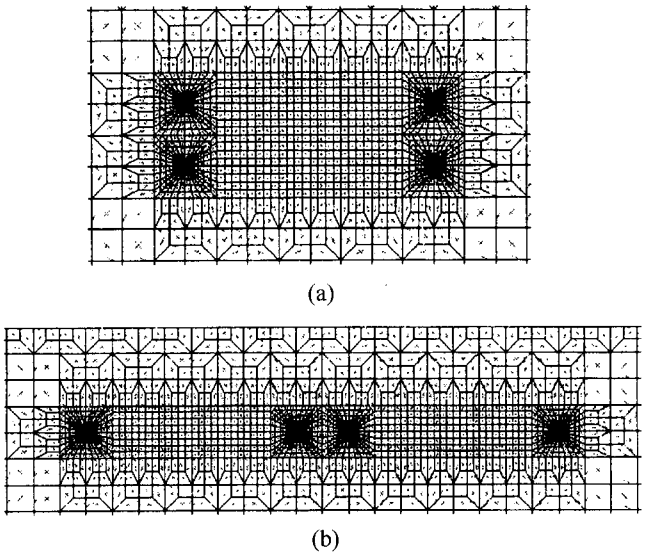

(a)

(b)

Fig. 3. Finite element mesh around. (a) parallel crack (b) coplanar crack.

indentation distance of 0.3 μm. The friction coefficient between the asperity and the half-space varied within a range of 0.1~1.0. Horizontal cracks with a length of 2c = 8 μm were modeled at a depth of d = 4 μm and the distance from the adjacent crack was fixed at l = 2 μm. A homogeneous isotropic elastic half-space with a Young's modulus of 310 GPa and Possion's ratio of 0.29 was assumed to have a material property such as Si_3N_4.

Finite Element Model

Fig. 2 shows a finite element model of a half-space. The MARC finite element program was used to create the model. The finite element mesh, 200 μm long and 160 μm wide (226 μm long and 160 μm wide for coplanar crack), consisted of 2899~3551 isoparametric eight-node quadrilateral plane-strain elements. Figs. 3 (a) and (b) illustrate the details of the mesh around the crack tip. The mesh around the crack consisted of eight-node collapsed quadrilateral plane strain

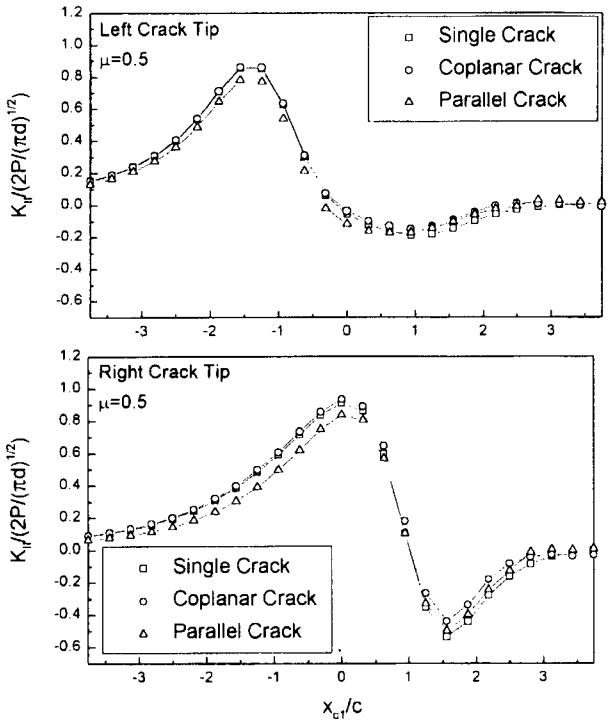

Fig. 4. Variation of dimensionless K_{II} with asperity position and contact friction for μ=0.5.

elements with the mid-side nodes adjacent to the crack tips displaced to a quarter-point distance, in order to simulate the singularity of the crack-tip stress field [7-9]. The nodes at each crack tip were constrained to move together so that no material overlap or crack tip blunting could occur at the crack tips [10]. The nodes at the bottom boundary of the mesh were constrained against displacement in the vertical direction, whereas the left and right corner nodes were constrained against displacement in the horizontal direction.

Results and Discussion

Calculation of Stress Intensity Factor

The mode I and mode II stress intensity factors are defined as

$$K_I = \lim_{r \to 0} \sqrt{2\pi r}\,\sigma_{yy} \quad (r, \theta) \tag{1}$$

$$K_{II} = \lim_{r \to 0} \sqrt{2\pi r}\,\tau_{xy} \quad (r, \theta) \tag{2}$$

where (x,y) and (r,θ) are the cartesian and cylindrical coordinates centered at the crack tip, respectively (see Fig. 1). The KI and KII values were determined by using a linear extrapolation to r = 0 [11]. The error was checked by solving a simple problem. A comparison between the finite element and analytical results showed differences of less than 2.8%. Hence, it would appear that the proposed finite element mesh and method of calculating the stress intensity factor are appropriate for analyzing the sliding of an asperity on a semi-infinite half-space. The resulting data were normalized using $2P/(\pi d)^{1/2}$.

The variation in the stress intensity factors for single,

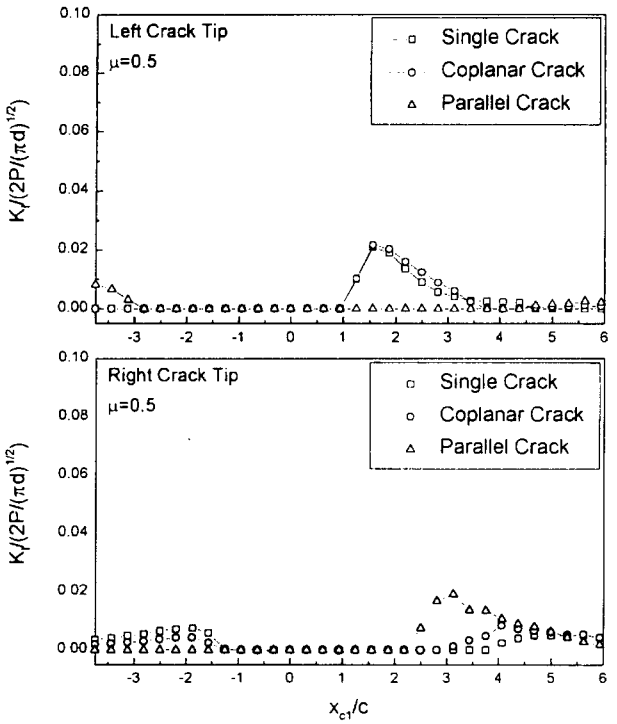

Fig. 5. Variation of dimensionless K_I with asperity position and contact friction for μ=0.5.

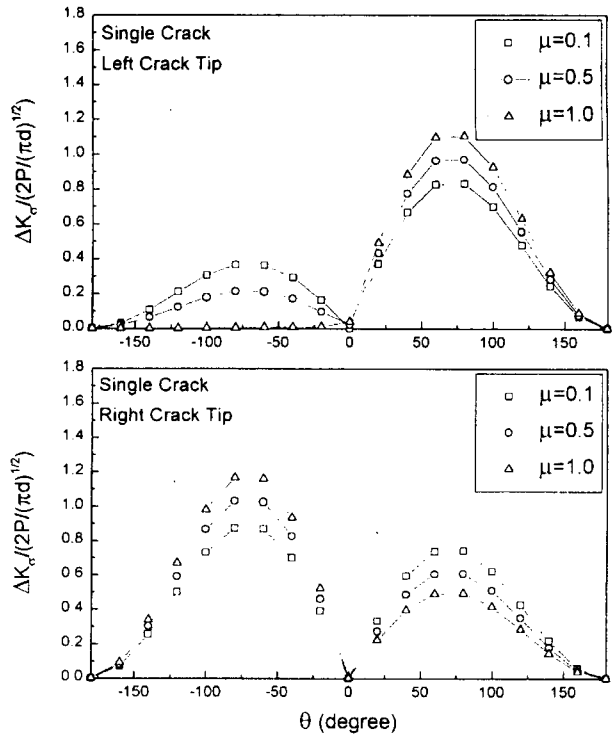

Fig. 6. Variation of dimensionless $\Delta K\sigma$ relative to direction and contact friction.

coplanar, and parallel cracks at the left crack tip in the case of a friction coefficient of 0.5 are shown in Fig. 4.

The maximum and minimum values of KII occurred before and after the asperity was over the tip. When compared with a single crack, the interaction of a coplanar crack increased the stress intensity factor. However, with a parallel crack, the stress intensity factor was reduced. These trends were more obvious at the right crack tip. Fig. 5 shows the variation of KI relative to the asperity position. KI was much smaller than KII. There was a small difference in the stress intensity factor between the single, coplanar and parallel cracks.

Crack Growth Direction

The contact between two surfaces can be thought of as the number of asperity contacts. Their relative motion results in a cyclic variation of the stress in the material. Hence, the crack growth is a fatigue process and can be assumed to occur in the plane of either the maximum shear stress intensity factor range or the maximum tensile stress intensity factor range [6]. The two-dimensional stress field in the vicinity of the crack tip can be given by [2,6,15]

$$\sigma_r = \frac{1}{\sqrt{2\pi r}}\cos\frac{\theta}{2}\left[K_I\left(1+\sin^2\frac{\theta}{2}\right)+K_{II}\left(\frac{3}{2}\sin\theta-2\tan\frac{\theta}{2}\right)\right] \quad (3)$$

$$\sigma_\theta = \frac{1}{\sqrt{2\pi r}}\cos\frac{\theta}{2}\left[K_I\cos^2\frac{\theta}{2}-K_{II}\sin\theta\right] \quad (4)$$

$$\tau_{r\theta} = \frac{1}{\sqrt{2\pi r}}\cos\frac{\theta}{2}[K_I\sin\theta+K_{II}(3\cos\theta-1)] \quad (5)$$

Introducing the tensile and shear stress intensity factor and their ranges [6],

$$K_\sigma(\theta, x_{c1,2}/c) = \sigma_\theta\sqrt{2\pi r}$$
$$K_\tau(\theta, x_{c1,2}/c) = \tau_{r\theta}\sqrt{2\pi r} \quad (6)$$

$$\Delta K_\sigma = \Delta K_\sigma(\theta) = K_{\sigma,max}\big|_{\theta=\theta^*} - K_{\sigma,min}\big|_{\theta=\theta^*}$$
$$\Delta K_\tau = \Delta K_\tau(\theta) = K_{\tau,max}\big|_{\theta=\theta^*} - K_{\tau,min}\big|_{\theta=\theta^*} \quad (7)$$

where subscripts max and min denote the maximum and minimum values of Kσ and Kτ. The maximum tensile and shear stress intensity factor ranges are given by

$$(\Delta K_\sigma)_{max} = max(\Delta K_\sigma) \qquad -180° \le \theta \le 180°$$
$$(\Delta K_\sigma)_{max} = max(\Delta K_\sigma) \quad (8)$$

Crack Propagation Angle

Figs. 6 and 7 show the variation in the dimensionless $\Delta K\sigma$ and $\Delta K\tau$ relative to direction and contact friction. The maximum values of $\Delta K\tau$ at both tips occurred at $\theta = 0°$, whereas those of $\Delta K\sigma$ at the left and right tips occurred at $\theta = 71.37°$ and $\theta = -70.5°$, respectively. These values are in good agreement with the results of K.Komvopoulus at $\theta = 70.5°$ and $\theta = -70.5°$.

When the shear mechanism was dominant, the crack propagated along the crack plane. However, when the tensile mechanism was dominant, the propagation from the left tip tended to occur toward the surface and that from the right tip proceeded downward into the half-space. The results for the

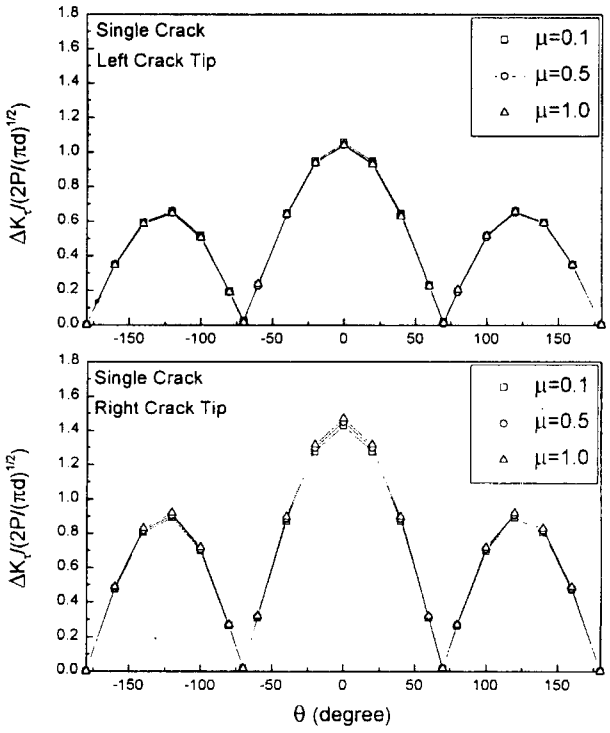

Fig. 7. Variation of dimensionless $\Delta K\tau$ relative to direction and contact friction.

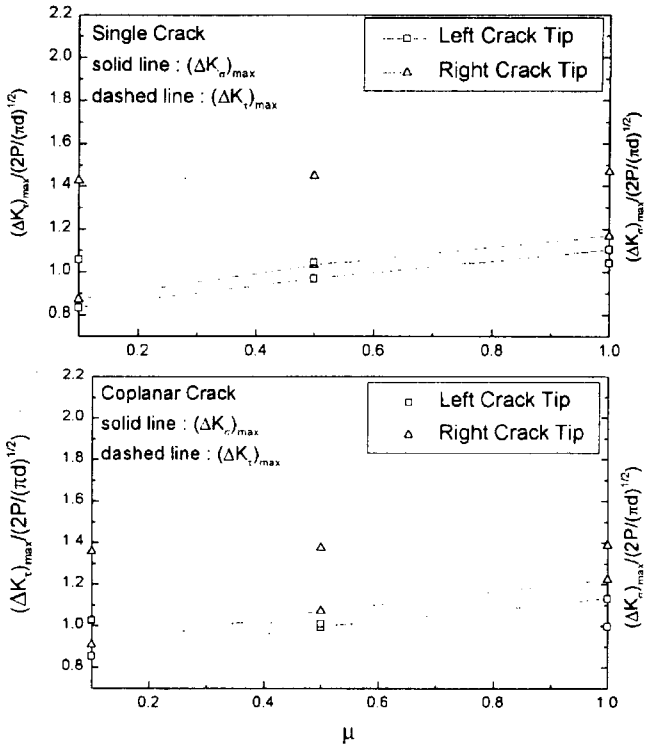

Fig. 8. Variation of dimensionless $(\Delta K\sigma)_{max}$ and $(\Delta K\tau)_{max}$ relative to contact friction for single and multiple cracks.

multiple cracks were found to have the same trends as those shown in Figs. 6 and 7. The interaction between the cracks did not seem to have much influence on the crack propagation angle.

Fig. 8 shows the variation in the dimensionless $(\Delta K\tau)_{max}$ and $(\Delta K\sigma)_{max}$ relative to the contact friction for single and multiple cracks. This figure shows that for a low friction coefficient, $(\Delta K\tau)_{max} > (\Delta K\sigma)_{max}$. However, as the friction coefficient increased, $(\Delta K\sigma)_{max}$ became higher than $(\Delta K\tau)_{max}$. At the right tip, $(\Delta K\tau)_{max}$ was always greater than $(\Delta K\sigma)_{max}$. In comparison with of Fig. 8, $(\Delta K\sigma)$ increased with a coplanar crack, whereas the opposite occurred with a parallel crack. In addition, Fig. 8 illustrates that the stress intensity factor at the right tip was generally greater than that at the left tip. This means that the crack growth at the right tip was faster.

According to these results, with a low initial friction coefficient, a subsurface crack will propagate along the crack plane, however, as the friction coefficient increases, the tensile mechanism becomes dominant and the propagation from the left tip will tend to occur toward the surface whereas in-plane crack growth will still occur at the right tip.

Conclusion

An analysis of multiple subsurface crack propagation in a half-space due to sliding contact was performed using the finite element method. With a coplanar crack, the stress intensity factor was increased. However, with a parallel crack, the stress intensity factor was decreased. The interaction between the cracks did not have much influence on the crack propagation angle. These results indicate that the interaction of a coplanar crack increases fatigue crack propagation, whereas that of a parallel crack decreases it.

Acknowledgment

This reseach was studied by the financial support of Korea research Foundation made in the program year of 1997 (1997-011-E00024).

Nomenclature

c	half-crack length
d	crack depth
l	distance between two cracks
μ	friction coefficient
ν	Possions ratio
E	Youngs modulus
P	maximum hertian contact pressure
r	crack tip radial polar coordinate
θ	crack tip angular polar coordinate
x_{c1}, x_{c2}	asperity distance from crack center
K_I, K_{II}	mode I and mode II stress intensity factors
K_s, K_t	tensile and shear stress intensity factors
$K_{s,max}$, $K_{t,max}$	maximum tensile and shear stress intensity factors
$K_{s,min}$, $K_{t,min}$	minimum tensile and shear stress intensity factors
ΔK_I, ΔK_{II}	mode I and mode II stress intensity factor

ranges

ΔK_s, ΔK_t tensile and shear stress intensity factor ranges

$(\Delta K_s)_{max}$, $(\Delta K_t)_{max}$ maximum tensile and shear stress intensity factors

References

1. Suh, N. P., The Delamination Theory of Wear, Wear, vol. 25, pp. 111-124, 1973.
2. Suh, N. P., Tribophysics, Prent ice-Hall, First Edition, 1986.
3. Shin, H. C., Suh, N. P., Subsurface Crack Propagation Due to Surface Traction in Sliding Wear, Journal of Applied Mechanics, vol. 51, pp. 317-322, 1984.
4. Salehizadeh, N., Saka, N., Crack Propagation in Rolling Line Contacts, ASME Journal of Tribology, vol. 114, pp. 690-697, 1992.
5. Jayaraman, S., Sadeghipour, K. and Baran, G., Finite Element Analysis of Horizontal and Branched subsurface Cracks in Brittle Materials, Wear, vol. 208, pp. 237-242, 1997.
6. Komvopoulos, K., Cho, S. S., Finite Element Analysis of Subsurface Crack Propagation in a Half-space Due to a Moving Asperity Contact, Wear, vol. 209, pp. 57-68, 1997.
7. Bath, K. J., Finite Element Procedures. Prentice-Hall, 1996.
8. Cook, R. D., Malkus, D. S. and Plesha, M. E., Concepts and Applications of Finite Element Analysis. Third Edition, John Wiley & Sons, 1989.
9. Aliabadi, M. H., Rooke, D. P., Numerical Fracture Mechanics. First Edition, Kluwer Academic Publishers, 1991.
10. Anderson, T. L., Fracture mechanics; Fundamentals and Application, Second edition, CRC Press, 1995.
11. David Broek, Elementary Engineering Fracture mechanics, Sijthoff & Noordhoff, 1978.
12. Fernand Ellyin, Fatigue Damage Crack Growth and Life Prediction, First Edition, Champman & Hall, 1997.